Supporting Information

Multiple synergistic strategy to Fabricate Si@TiO_2/C-ZIF-8@CNFs with Hierarchical Porous for enhancing Li storage kinetics

Chentong Guo[a], Zhiyuan Gao[a], Songchen Zheng[a], Junhao Zhang[a,*], Qianqian Fan[a], Xingmei Guo[a], Yuanjun Liu[a], Xiangjun Zheng[a], Zhongyao Duan[a], Shenglin Xiong[b,*]

[a]School of Environmental and Chemical Engineering, Jiangsu University of Science and Technology, Zhenjiang, Jiangsu, 212003, China

[b]School of Chemistry and Chemical Engineering, State Key Laboratory of Crystal Materials, Shandong University, Jinan, Shandong 250100, China

Corresponding Authors: jhzhang6@just.edu.cn (J. Zhang); chexsl@sdu.edu.cn (S. Xiong)

Experimental section

Chemicals

All chemicals are analytical reagent grade and do not require further purification. Si nanoparticles (80 nm, 99.99%) were obtained from Hebei Xintie Metal Materials Co., Ltd. butyl titanate ($C_{16}H_{36}O_4Ti$, CP), zinc nitrate hexahydrate ($Zn(NO_3)_2{\cdot}6H_2O$, AR), 2-methylimidazole ($C_4H_6N_2$, 98%), N, N-dimethylformamide (DMF, AR), ammonia solution ($NH_3{\cdot}H_2O$, AR), polyacrylonitrile (PAN, average Mw=150,000), sodium carboxymethyl cellulose (CMC, CP) were supplied by China National Pharmaceutical Group Shanghai Co., Ltd. Carbon black (Super P, AR) were obtained from Lion Corporation, electrolyte (1.0M LiPF6 in EC:DEC=1:1 vol% with 5.0%FEC) were obtained from Canrd Technology Co.Ltd., Li sheet(16*0.6mm) were obtained from Zhenjiang Longda Chemical Reagent Packaging Co., Ltd.

Preparation of Si@TiO_2 composite

First, 0.2 g Si nanoparticles was added to a 500 mL beaker containing 270 mL anhydrous ethanol and 0.8 mL ammonia solution. The mixture was ultrasonicated for 30 min to achieve a uniformly dispersed suspension. Subsequently, the suspension was stirred at 45 °C for 30 min, followed by the dropwise addition of 2 mL tetrabutyl titanate. The coating process was carried out by maintaining the temperature at 45 °C under continuous stirring for 24 h. The resulting product was collected via centrifugation, washed repeatedly with anhydrous ethanol to remove residual reactants, and dried at 60 °C for 8 h, which was named as Si@TiO_2.

Preparation of ZIF-8 nanocrystals

Two 250 mL beakers were each filled with 100 mL anhydrous methanol. Subsequently, 2.3 g $Zn(NO_3)_2{\cdot}6H_2O$) and 5.1 g 2-methylimidazole were added into the above different beakers, respectively. Each mixture was magnetically stirred for 15 min to ensure complete dissolution. The two solutions were then combined under vigorous stirring for 20 min, followed by aging at room temperature for 2 h. The resulting precipitate was collected by centrifugation, washed repeatedly with methanol to remove unreacted reagents, and dried at 60 °C for 10 h, obtaining ZIF-8

powder.

Preparation of Si@TiO_2/C-ZIF-8@CNFs composite

1.0 g PAN was dissolved in 10 mL N, N-dimethylformamide under magnetic stirring at 50 °C until a transparent solution was obtained. Subsequently, 0.1 g Si@TiO_2 nanoparticles and 1.0 g ZIF-8 particles were dispersed into the PAN solution and vigorously stirred for 24 h to form homogeneous electrospinning dispersion. The dispersion was loaded into a 10 mL syringe equipped with a single-nozzle spinneret. Electrospinning was conducted at 25 °C with the following parameters: a working voltage of 17 kV, a syringe pump flow rate of 0.01 mL min^{-1}, a collector rotation speed of 400 rpm, and a tip-to-collector distance of 15 cm. To preserve the fibrous morphology, the as-spun Si@TiO_2/ZIF-8@PAN precursor was stabilized in a muffle furnace at 250 °C for 1 h under air. Subsequently, the stabilized fibers were carbonized under Ar atmosphere at 800 °C for 2 h (heating rate of 5 °C min^{-1}) to obtain Si@TiO_2/C-ZIF-8@CNFs composite. Aiming to contrast the electrochemical properties of the Si@TiO_2/C-ZIF-8@CNFs composite, Si@TiO_2@CNFs composite was additionally prepared.

Characterization

The morphology and internal structure of samples were examined via scanning electron microscopy (SEM, JEOL JSM-7500F) and transmission electron microscopy (TEM, JEOL-2100F). The phase and composition of Si@TiO_2/C-ZIF-8@CNFs, Si@TiO_2 and Si@TiO_2@CNFs composites were analyzed by using X-ray diffraction (XRD-6000, Cu target: λ=1.5418 Å, scan angle range of 10 to 80°, sweep speed of 5°min^{-1}). To record the chemical states and binding energy of surface elements, X-ray photoelectron instrument (XPS, Thermo Fisher Scientific Escalab-250 Xi) was employed to test the samples. The graphitization degree of Si@TiO_2/C-ZIF-8@CNFs and Si@TiO_2@CNFs composites were measured by Raman spectroscopy (Edinburgh RM5, λ=514 nm).

Electrochemical measurements

For the electrochemical investigation, the working electrode was fabricated using Si@TiO_2/C-ZIF-8@CNFs composite, while a high-purity lithium foil served as the counter electrode to construct a half-cell configuration. For electrode preparation, the active material (Si@TiO_2/C-ZIF-8@CNFs), conductive carbon black (Super-P), and sodium carboxymethyl cellulose (CMC) binder were mechanically blended and ground at a mass ratio of 7:2:1 for 30 min. An appropriate amount of deionized water was then added to the mixture, which was stirred continuously for 12 h to form homogeneous rheological slurry. The slurry was uniformly coated onto a copper foil current collector and dried overnight in a vacuum oven at 60 °C. The mass loading of active material on the electrode was controlled at approximately 1.0 mg cm^{-2}. A Celgard 2400 polypropylene membrane was employed as the separator, and the electrolyte consisted of 1.0 mol L^{-1} lithium hexafluorophosphate ($LiPF_6$) dissolved in a mixed solvent of ethylene carbonate (EC), dimethyl carbonate (DMC), and diethyl carbonate (DEC) with a volume ratio of 1:1:1. All cell components were assembled into CR2032-type coin cells within an argon-filled glovebox (H_2O and O_2 levels < 0.1 ppm). A total of 100 μL of electrolyte was added to each CR2032 coin-type cell during assembly.

The cyclic voltammetry (CV) curves were carried out on an electrochemical workstation, within a defined voltage window of 0.01-3.0 V. Meanwhile, the electrochemical impedance (EIS) of prepared substances was also investigated with frequency range configured from 1×10^{-2} to 1×10^{5} Hz. The detailed electrochemical performances of LIBs were precisely recorded by a LAND CT2001A battery tester. The Galvanostatic Intermittent Titration Technique measurements were carried out on the identical device. The batteries underwent testing for 30 min under a current flux and were then allowed to rest in an open-circuit state for 150 min. This process was repeated to attain a steady state at a current density of 100 mA g^{-1} within the voltage range from 0.01 to 3.0 V.

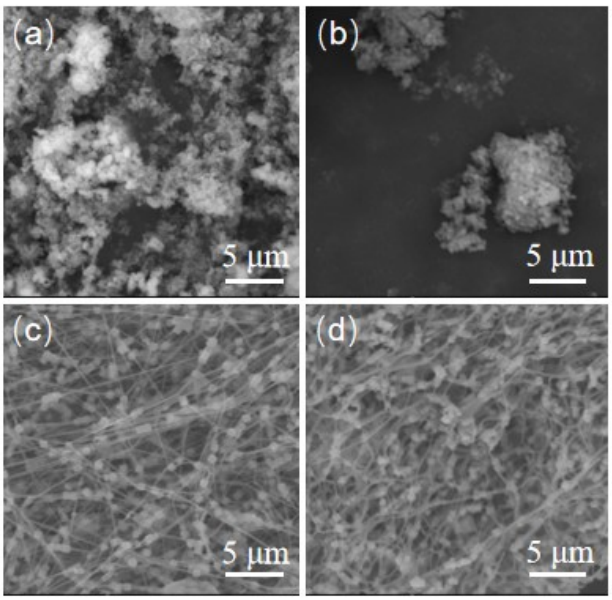

Fig. S1. SEM images: (a)Si@TiO_2; (b) ZIF-8 nanocrystals; (c) Si@TiO_2/C-ZIF-8@PAN; (d) Pre-oxidized Si@TiO_2/C-ZIF-8@PAN.

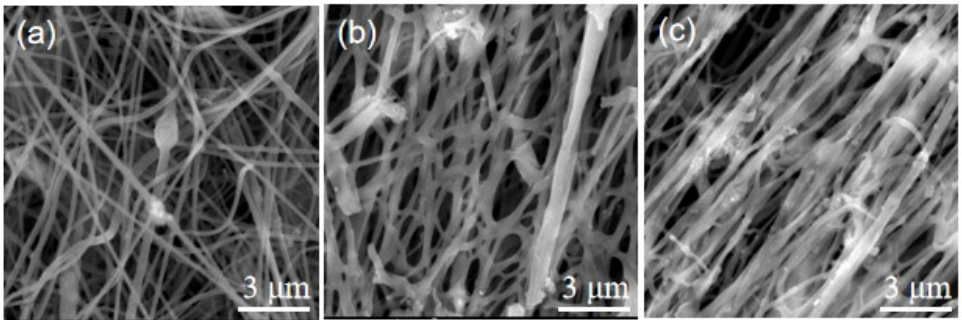

Fig. S2. SEM images: (a) Si@TiO_2@PAN; (b) Pre-oxidized Si@TiO_2@PAN; (c) Si@TiO_2@CNFs.

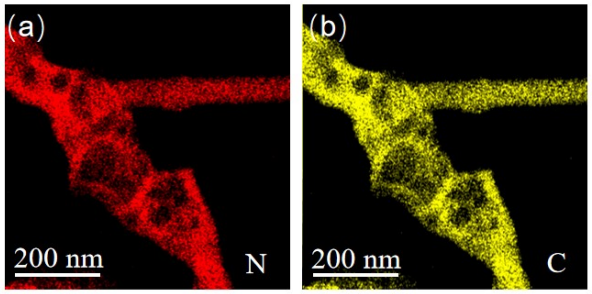

Fig. S3. Elemental mapping images of the Si@TiO_2/C-ZIF-8@CNFs: (a) N; (b) C.

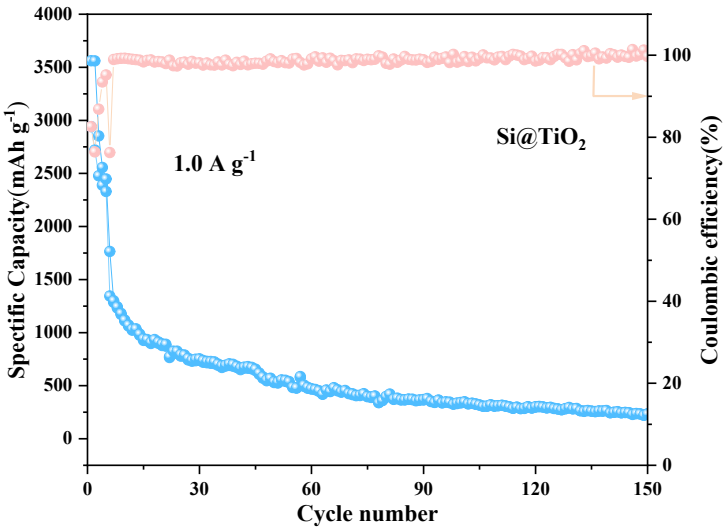

Fig. S4. Cycling performance of Si@TiO_2 anode at 1.0 A g^{-1}.

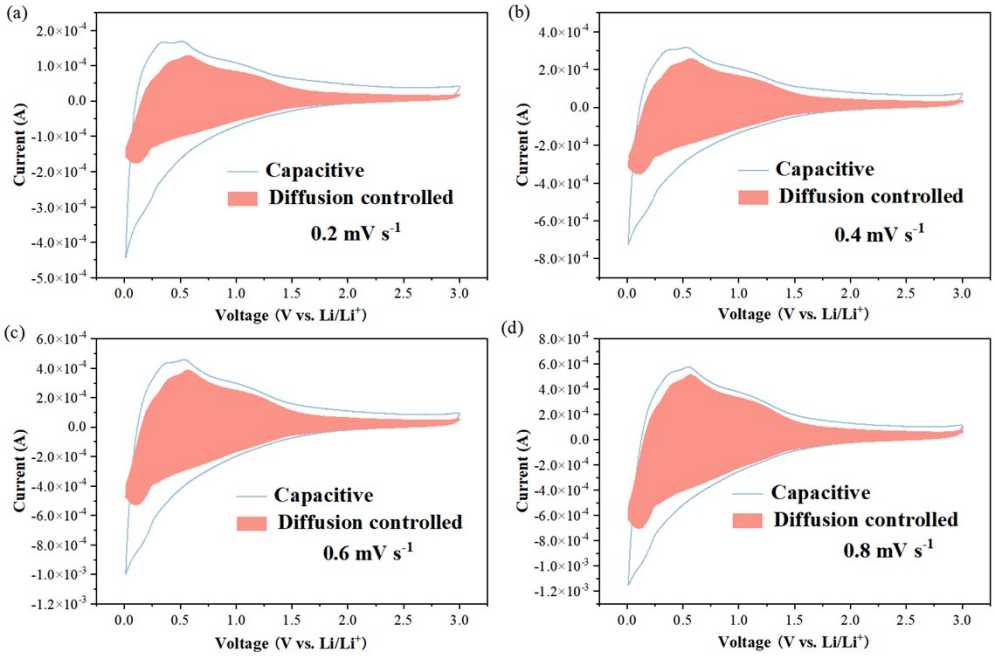

Fig. S5. Capacitance contribution of Si@TiO_2/C-ZIF-8@CNFs anode: (a) 0.2 mV s^{-1}; (b) 0.4 mV s^{-1}; (c) 0.6 mV s^{-1}; (d) 0.8 mV s^{-1}.

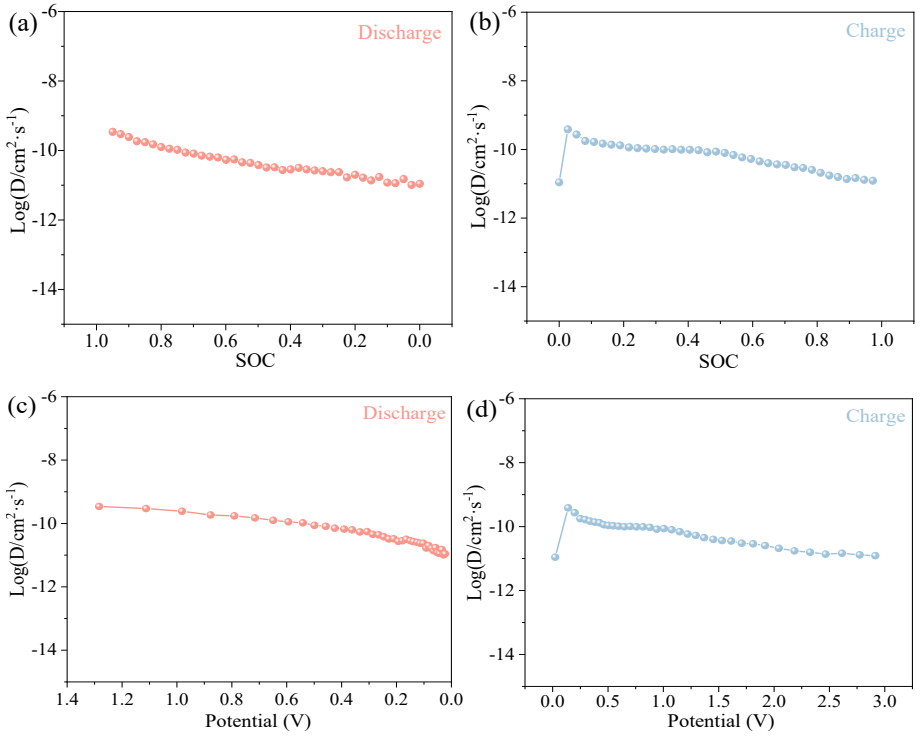

Fig. S6. (a, b) Relationship between D_{Li}^+ and SOC during discharge and charging; (c, d) Relationship between D_{Li}^+ and voltage during discharge and charging.

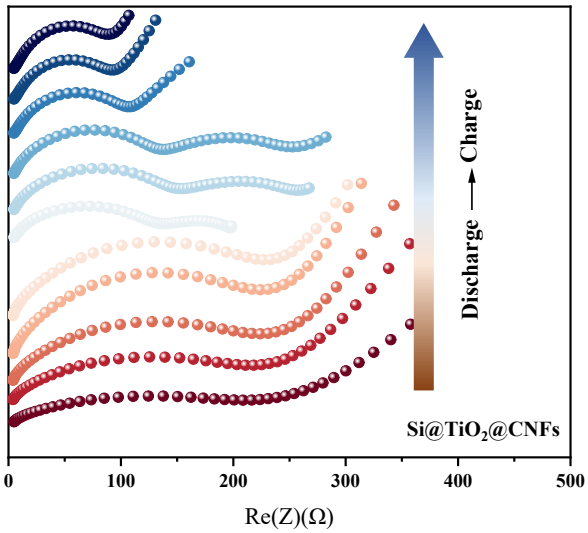

Fig. S7. In-situ impedance diagram of Si@TiO_2@CNFs anode

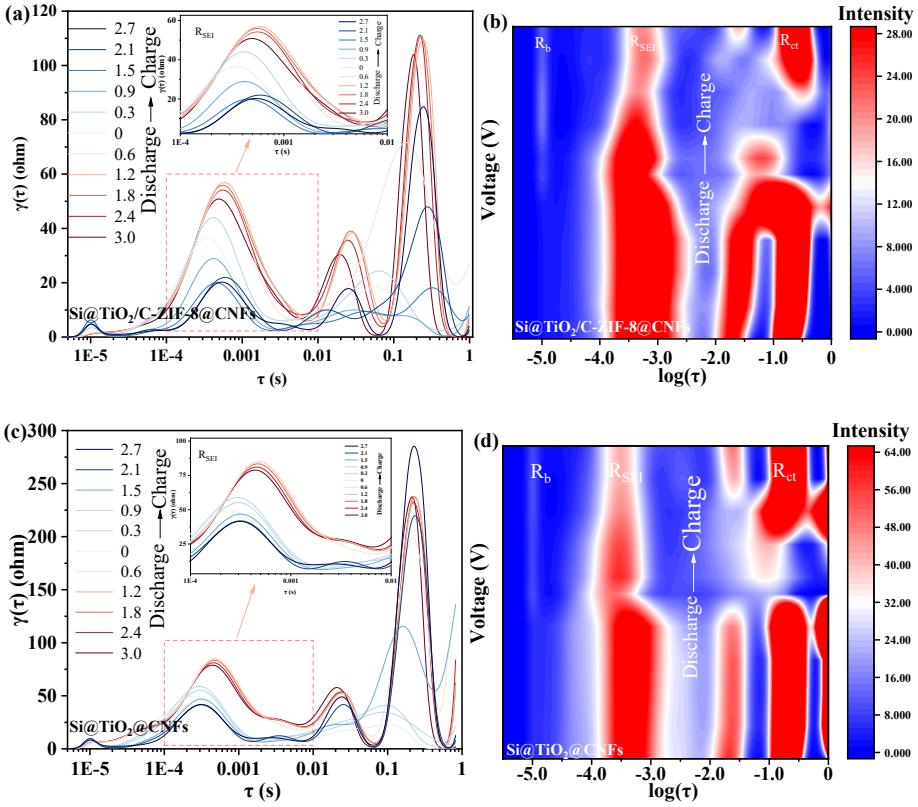

Fig. S8. Distribution of relaxation times (DRT) curve and its contour plot EIS of (a-b) Si@TiO_2/C-ZIF-8@CNFs and (c-d) Si@TiO_2@CNFs.

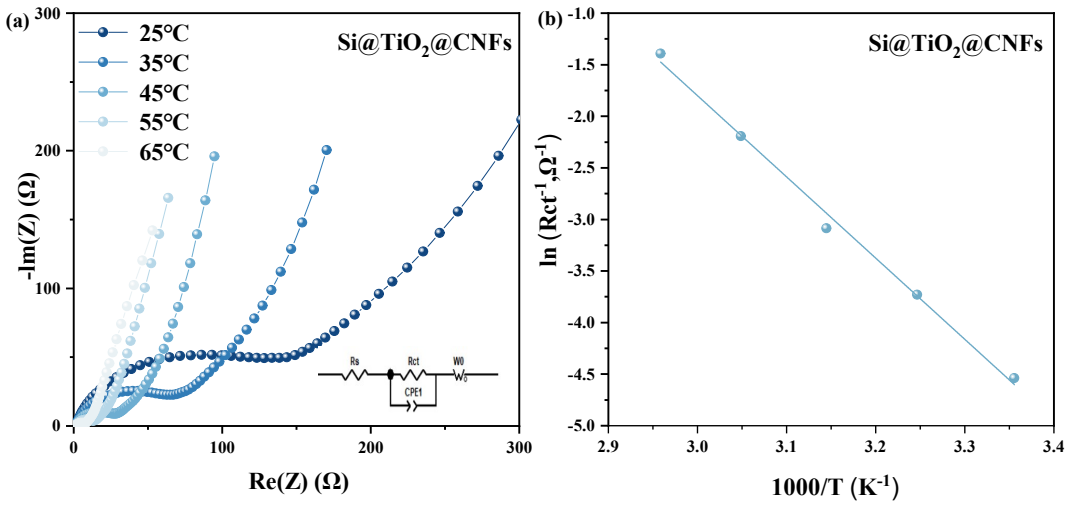

Fig. S9. (a) The temperature dependent impedance plots of Si@TiO_2@CNFs anode; (b) The Arrhenius plot of ionic conductivity versus temperature of Si@TiO_2@CNFs anode.

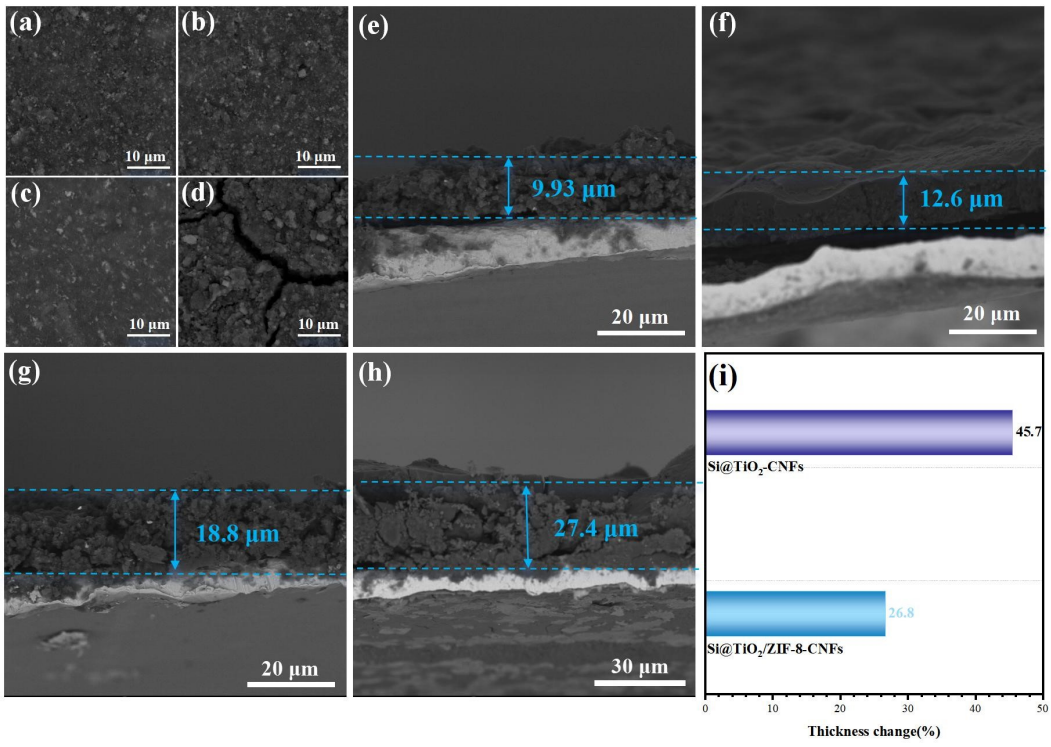

Fig. S10. (a, b) SEM images of Si@TiO_2/C-ZIF-8@CNFs anode before and after cycling; (c, d) SEM images of Si@TiO_2@CNFs anode before and after cycling; (e, f) Cross-sectional SEM images of Si@TiO_2/C-ZIF-8@CNFs anode before and after cycling; (g, h) Cross-sectional SEM images of Si@TiO_2@CNFs anode before and after cycling; (i) Comparison of thickness change of Si@TiO_2/C-ZIF-8@CNFs and Si@TiO_2@CNFs anodes before and after cycling.

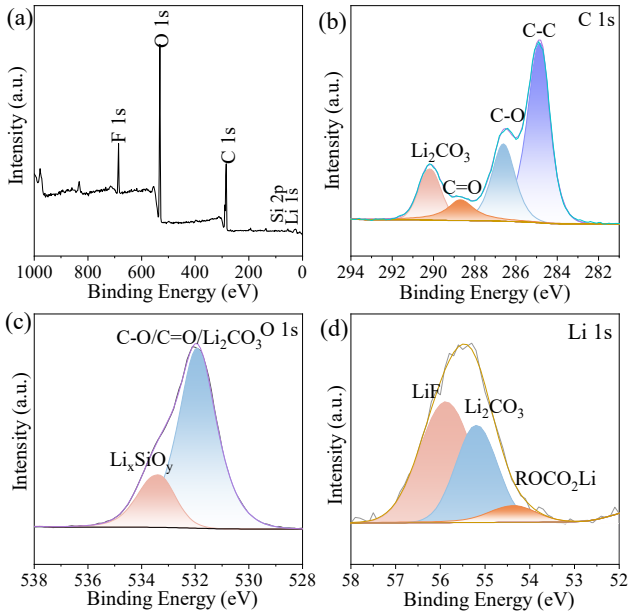

Fig. S11. (a) XPS survey spectrum of Si@TiO_2/C-ZIF-8@CNFs after the cycle; (b) High-resolution XPS spectrum of C 1s; (c)High-resolution XPS spectrum of O 1s; (d) High-resolution XPS spectrum of Li 1s.

Table S1. Comparisons of selected performance metrics of Si-based LIBs anodes

Anode materials	Current density ($mA\ g^{-1}$)	Cycle number	Reversible capacity ($mAh\ g^{-1}$)	Refs.
Si-C/TiO_2	800	900	919.8	[S1]
Si@TiO_2@rGO	500	400	1228.7	[S2]
carbon@TiO_2@Si	1000	200	372.0	[S3]
TiO_2/SiOx/Si	200	100	682.0	[S4]
SiNPs@TiO_2/AgNWs	1000	100	1157.6	[S5]
Si-TiO_2	1000	500	616.3	[S6]
TiO_2/Si/C	100	80	538.0	[S7]
Graphite/Si@TiO_2	500	100	506.2	[S8]
Si/s-C@TiO_2	200	100	780.0	[S9]
Si@C/TiO_2@C/Hollow-C	1000	400	558.0	[S10]
Si/TiO_2/PDA	500	175	934.8	[S11]
YS-Si/SiO_2-Ti@C	800	200	1290	[S12]
PSi@C@ TiO_2	500	250	1041	[S13]

$Si/TiO_2/rGO$	200	200	1333.8	[S14]
$Si@C@TiO_2$	1000	100	1618.2	[S15]
$Si@TiO_2$/C-ZIF-8@CNFs	**1000**	**500**	**754.1**	**This work**

References

S1. C. Xu, L. Shen, W. Zhang, Y. Huang, Z. Sun, G. Zhao, Y. Lin, Q. Zhang, Z. Huang, J. Li, Energy Storage Mater., 2023, 56, 319–330.

S2. Z. Wang, Z. Xu, Y. Yuan, X. Teng, Z. Pu, Y. Wang, A. Fu, Y.-G. Guo, H. Li, Appl. Surf. Sci., 2022, 598, 153790

S3. K. Wang, N. Li, J. Xie, G. Lei, C. Song, S. Wang, P. Dai, X. Liu, J. Zhang, X. Guo, Electrochim. Acta, 2021, 372, 137863.

S4. J. Li, Y. Li, J. Shi, H. Liu, D. Wang, W. Zhai, Z. Meng, Colloids Surf. Physicochem. Eng. Asp., 2021, 625, 126870.

S5. J. Li, S. Fan, H. Xiu, H. Wu, S. Huang, S. Wang, D. Yin, Z. Deng, C. Xiong, Nanomaterials, 2023, 13, 1144.

S6. Y. Huang, Y. Lv, Y. Zou, N. Chen, Z. Ao, J. Electroanal. Chem., 2023, 930, 117128.

S7. S. Xie, Q. Ji, Y. Xia, K. Fang, X. Wang, X. Zuo, Y. Cheng, ChemistrySelect, 2021, 6, 141–153.

S8. B. N. Vats, R. Gupta, A. Gupta, S. Fatima, D. Kumar, ChemistrySelect**,** 2024, 9, e202303545.

S9. X. Chen, J. Zheng, L. Li, W. Chu, RSC Adv., **2022**, 12, 17889–17897.

S10. Y. Li, G. Chen, J. Lin, L. Huang, C. Zhang, X. Luo, ACS Appl. Energy Mater., 2021, 4, 14526–14536.

S11. L. Chen, L.-Q. Fan, F.-F. Deng, L.-N. Wang, X.-Y. Song, X.-T. Zhu, F.-D. Yu, Y.-F. Huang and J.-H. Wu, *Electrochimica Acta*, 2025, **538**, 146997.

S12. Y. Li, S. Sun, J. Tang, S. Han, Y. Yang, J. Xing, L. Zong, L. Wang and B. Li, *Nano Research*, 2024, **18**, 94907474.

S13. J. Luo, P. Xiao, Y. Li, J. Xiong, P. Zhou, L. Pang, X. Xie and Y. Li, *Dalton Trans.*, 2023, **52**, 2463–2471.

S14. P. Su, Y. Zhou, J. Wu, J. Shao, L. Shen and N. Bao, *Ind. Eng. Chem. Res.*, 2024, **63**, 1422–1431.

S15. B. Ma, F. Xue, Z. Wang, L. Zhang, Z. Zhang, M. Chen, H. Zhu, S. Lan, *Prog. Nat. Sci.*, 2026, S1002007126000262.